Comparison of the Linear Finite Element Prediction of Deformation and Strain of Human Cancellous Bone to 3D Digital Volume Correlation Measurements

R. Zauel

Y. N. Yeni

Bone and Joint Center,
Department of Orthopaedic Surgery,
Henry Ford Health System,
Detroit, MI 48202

B. K. Bay
Oregon State University,
Corvallis, OR 97331

X. N. Dong

D. P. Fyhrie[1]

Bone and Joint Center,
Department of Orthopaedic Surgery,
Henry Ford Health System,
Detroit, MI 48202

The mechanical properties of cancellous bone and the biological response of the tissue to mechanical loading are related to deformation and strain in the trabeculae during function. Due to the small size of trabeculae, their motion is difficult to measure. To avoid the need to measure trabecular motions during loading the finite element method has been used to estimate trabecular level mechanical deformation. This analytical approach has been empirically successful in that the analytical models are solvable and their results correlate with the macroscopically measured stiffness and strength of bones. The present work is a direct comparison of finite element predictions to measurements of the deformation and strain at near trabecular level. Using the method of digital volume correlation, we measured the deformation and calculated the strain at a resolution approaching the trabecular level for cancellous bone specimens loaded in uniaxial compression. Smoothed results from linearly elastic finite element models of the same mechanical tests were correlated to the empirical three-dimensional (3D) deformation in the direction of loading with a coefficient of determination as high as 97% and a slope of the prediction near one. However, real deformations in the directions perpendicular to the loading direction were not as well predicted by the analytical models. Our results show, that the finite element modeling of the internal deformation and strain in cancellous bone can be accurate in one direction but that this does not ensure accuracy for all deformations and strains. [DOI: 10.1115/1.2146001]

Introduction

It has become common to study the mechanical properties of whole bones using finite element models (FEM) created from high resolution computed tomography and magnetic resonance images taken at a resolution compatible with in vivo scanning [1–10]. For higher resolution modeling of mechanical behavior, images are obtained that resolve the individual trabeculae of cancellous bone tissue and from these images finite element models are made and solved to estimate the strain, stress, and deformation fields of the individual trabeculae [4,11–19]. At all levels of resolution, the finite element method has proven itself to be a very useful tool to understand and predict the mechanical properties of both whole bones and bone tissue. As examples, linear FEM estimation of bone modulus predicts more than 80% of the variance in experimental modulus and strength of cancellous bone specimens [12,17] and is applicable to tracking changes in bone mechanical properties in vivo [5,16]. Developing an empirical approach to testing the predictions of the finite element method could result in even better predictions than are already available.

To test the strain predictions of FEM experimentally, it has traditionally been necessary to mechanically test bones in vitro and compare measured strains [20–22] to a finite element simulation of the experiment. However, strain gages and markers only measure surface strain, which leaves FEM predicted internal deformations of bone untested. As a consequence of the limitation of strain gages bonded to the surface of bone, the finite element predictions of deformation and strain in bone have never been directly compared to a full field of 3D measurements. We have developed an experimental method that can measure the 3D internal deformation of cancellous bone and estimate the 3D strain distribution [23–25]. The main goal of our current research was to compare linear FEM predictions against 3D experimental deformation and strain data for cancellous bone. Note that the inhomogenous 2D surface displacements of cancellous bone specimens have been measured [26] but that FEM predictions of cancellous bone deformation have never been directly compared to deformation data.

The digital volume correlation method (DVC) was devised to measure the 3D internal deformations of structures by comparing mechanically deformed and undeformed computed tomography images [24,25]. The DVC method is, essentially, a 3D version of the 2D methods of texture correlation [23] or photogrammetry [27] where the deformation of a surface is determined by correlating the texture of the deformed image to that of an undeformed image. In the DVC method a similar approach is applied to computed tomography scans where portions of the image are tracked between the deformed and undeformed scans to determine the vector field of deformations caused by a mechanical load. After the deformation field is measured, the strain field (based on derivatives of the deformation) can easily be computed.

In initial reports, DVC was used to measure the strain in cylin-

[1]Corresponding author: Director of Research, Lawrence J. Ellison Musculoskeletal Research Center, University of California, Davis, 4635 Second Avenue, Room 2000, Sacramento, CA 95817; phone: (916)734-5079.

Contributed by the Bioengineering Division of ASME for publication in the JOURNAL OF BIOMECHANICAL ENGINEERING. Manuscript received November 3, 2003; final manuscript received July 21, 2005. Review conducted by Lori A. Setton.

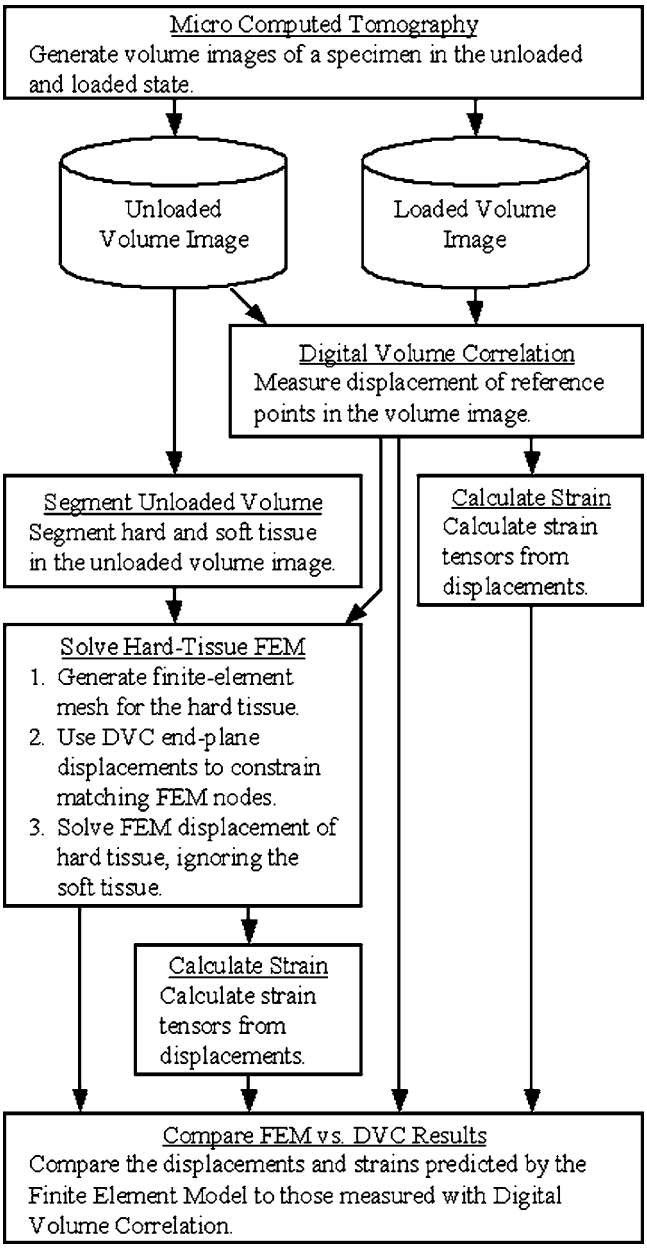

Fig. 1 Flowchart for the project

ders of cancellous bone deformed by a radiolucent mechanical loading system mounted in a microcomputed tomography system [24]. The precision of DVC for measuring the strain of cancellous bone specimens was, on average, better than 302 microstrain [24]. This reported precision would be sufficient to test FEM predictions to some degree; however, an improved strain precision would be preferable. As a secondary goal of the current project, modifications to the DVC technology were made to improve its measurement precision.

Methods

Overview. The predictions of the internal strain and deformation from linear FEM models of cancellous bone were compared to deformation and strain data measured from the same specimens using the method of digital volume correlation (DVC). An overall outline of the steps of the comparison is presented in Fig. 1, with detailed explanations of the methods for each step outlined below.

Digital Volume Correlation. The methods used in the current study are similar to those described in our initial presentation of the DVC method without rotational degrees of freedom [24]. In detail, however, there are changes in the algorithms used to solve the problems. These changes resulted in a significant improvement in the method's precision and accuracy and are included in the following discussion. The following presentation of methods is complete, but a fuller understanding can be obtained by examining both the current and previous work. As a general overview, the DVC method uses three-dimensional image processing methods to measure the change in position of the internal features of an object by comparing images of the undeformed and deformed object. The collection of changes in position (the displacement field) is then used to calculate a strain field for the object.

Image volumes were obtained from two 15 mm in diameter and 18 mm high cylindrical bone specimens (one each from a human distal femur and vertebral body) using a micro CT system [28] and a radiolucent mechanical loading system [24]. The CT scans were reconstructed into volumetric models $520\times520\times580$ in size. Each image voxel was encoded as a gray-scale, 16-bit integer representing a 35 μm cube. The cancellous bone specimens were glued to the compression platens and axially compressed using our specially built radiolucent loading system. (The compression direction for the experiment was the "z" or axial direction of the cylinder. A more complete discussion of sample handling and loading has been reported previously [24].) Pairs of image volumes were taken of each specimen, one in the unloaded and another in the loaded state. For testing of precision, two sequential images of a vertebral cancellous bone specimen were taken without loading. This pair of images was used to measure the inherent noise in the imaging and tracking system [24].

The images were filtered by subtracting a value equal to the mode of the frequency distribution of the density and setting any resulting negative values to zero. This eliminated much of the inherent (stochastic) noise in the CT of the marrow regions. The resulting voxel values were linearly transformed so that the final density histograms of both images had a mean density of 1000. This postprocessing of the images greatly reduced the effects of drift in the x-ray source intensity between imaging times, resulting in improved displacement and strain precision.

Displacement of the specimen under loading was measured at a grid of reference points in the unloaded volume by matching a spherical subvolume (a 30-voxel radius was used in the current study) surrounding each reference point to the loaded volume so as to minimize the sum of squared differences in density between corresponding voxels. The initial guess for the deformed position of the subvolume was determined using an exhaustive digital search. In this process, the subvolume was matched against all possible *whole voxel* deformations that the tissue might have undergone. Using a systematic method greatly reduces the complexity of the search algorithm compared to a gradient approach and is quite rapid on modern computing equipment. Successful search results were used to predict the deformations of neighboring sites to improve the search speed.

Resolving the deformations at the subvoxel level was facilitated by using tricubic interpolations of the density values. Density was interpolated as:

$$d(x,y,z)=\sum_{i=0}^{3}\sum_{j=0}^{3}\sum_{k=0}^{3}C_{ijk}x^iy^jz^k, \tag{1}$$

where x, y, and z are the coordinates within the unit cube. The 64 coefficients of Eq. (1) can be obtained by multiplying a 64-tuple of all voxels within one voxel space of the cube by a constant 64×64 transformation matrix (Appendix A). Matrix operations perform well in the four-way SIMD (single instruction multiple data) unit of a Pentium 4 PC and the coefficients were cached during the search process. The vector of 64 $x^iy^jz^k$ terms was precomputed for each search, and then multiplied in turn by the

cached coefficient vectors of each voxel position using SIMD arithmetic. This approach permitted rapid evaluation of candidate search locations. An empirically chosen limit on maximum distance traveled was used for each coordinate of displacement so as to reject reference points that failed to converge.

Subvoxel search was performed using a steepest descent algorithm [29] with a quadratic prediction heuristic. Using the results of the systematic search as an initial guess, the sum-of-squares fit function and its three partial derivatives were computed simultaneously with four-way SIMD. Four new guesses were chosen along the negative gradient line (0.5 voxel spaces, 0.01 voxel spaces, and two distances logarithmically spaced between them) and evaluated simultaneously with four-way SIMD. The three best fits were chosen among the original and four new guesses, and a parabola was used to predict the minimum fit position on the gradient line. This became the guess for the next iteration. The search ended when the distance moved was less than 0.01 voxel spaces. Searches typically converged in an average of 3.2 iterations.

To smooth the displacement data and to calculate the strain, a triquadratic function was fit to each displacement coordinate of each base reference point and its 60 closest neighbors ([24], Appendix B). If the displacement data were to be smoothed, the constant term of the function was used as the smoothed displacement of the base point. To determine the strain, the displacement data (either smoothed or unsmoothed) were fit by the triquadratic function and the coefficients of the linear terms were used to calculate the strain tensor. The matrix of coefficients for the quadratic terms is an estimate of the Jacobian matrix of the displacement field [30]. The linear strain tensor was calculated as the symmetric part of the Jacobian matrix.

Finite Element Modeling. Using our previously published methods, FEM was used to analyze the displacement and strain distribution in a voxel based model of the specimen with uniform hard tissue modulus and Poisson's ratio set to $\nu=0.3$ [12]. (Note that the effect of Poisson's ratio was tested by running a case with $\nu=0.45$. This large change in Poisson's ratio did not affect any conclusions made based on the data from the simulations.) To simulate the glued condition of the experimental specimens, the boundary displacements for the models were matched to the DVC measured displacements at the top and bottom of the specimen. This accounted for rotation and translation of the glued ends of the specimens—our prototype mechanical loading system was too flexible and the endplanes of the specimens did not move with a perfectly plane translation during loading. The FEM model had a resolution of 43.75 micrometers. For comparison purposes, the detailed FEM displacements were averaged over the hard tissue within a radius of 1.05 mm (this eliminates averaging the unknown displacements of the marrow) to reduce their resolution to be comparable to the displacement measurements of the DVC method. The strain field associated with the smoothed FEM displacement field was calculated using the same methods as those to calculate the strain for the experimental DVC displacement field.

Comparison of Results. The displacement and strain fields for both the DVC and the FEM estimates were analyzed using linear regression analysis. The expected outcome (for a perfect prediction) is a coefficient of determination of one, a slope of one and a zero intercept for each component. Visualizations of the various parameters were also used to obtain better understanding the regression results.

Results

The error of the improved DVC process was evaluated by measuring the displacement and strain between two CT scans of the same vertebral cancellous bone specimen (Table 1). The standard deviation of the displacement was 0.008 voxel spaces and the strain was 168 μ-strain units. Smoothing the displacements improved these figures to 0.005 voxel spaces and 69 μ-strain units.

Table 1 Standard deviation of DVC measurement of displacement (d; in voxel units) and strain (ε; microstrain) for each of the natural axes taken from repeat scans. The columns are calculations from: Unsmoothed (raw) DVC displacement data, from DVC data smoothed as described in the text and from the original report of the DVC method for these same image data [23].

Standard Deviation of Displacement (voxels)	Raw	Smooth	Bay et al. [23]
dx	0.009	0.006	0.031
dy	0.009	0.006	0.044
dz	0.007	0.004	0.030
d (average)	0.008	0.005	0.035
Standard Deviation of Strain (microstrain)			
ε_{xx}	279	100	457
ε_{yy}	224	87	323
ε_{zz}	131	66	280
ε_{xy}	155	73	211
ε_{xz}	116	49	239
ε_{yz}	100	39	224
ε (average)	168	69	289

Both values compare well to data reported in an earlier study [24]. In the remainder of this study, the smoothed displacement method (strain precision of 69 μ-strain) was used. The DVC program ran for 470 milliseconds per reference point on a 1.8 GHz PC, a fourteen-fold improvement from the previous method. The performance improvement resulted from newer hardware, the use of SIMD programming for the calculations and a technique for guessing the initial inter-voxel displacement by fitting a parabola to the adjacent integer locations

The FEM and DVC displacement and strain results were generally highly related (Table 2) with better coefficients of determination 1) between the displacements than for strains and 2) for the femoral (high density) than for the vertebral (low density) specimen. The value of Poisson's ratio was unimportant to the accuracy of the predictions (data not shown). The best coefficient of determination between experimental and computer prediction of the displacement (Table 2; Fig. 2) was for the direction of loading (u_z) for both specimens. There was a similar finding for the strain in the loading direction (ε_{zz}; Table 1; Fig. 3), however, the xz shear strain in the vertebral specimen was slightly better predicted by the experimental values than was the zz normal strain. For the parameters with the better coefficient of determination (r^2; Table 2), the regression slopes were close to one as would be expected if FEM is an accurate method for prediction of 3D deformation and strain in cancellous tissue. However, the slopes of the regressions for the transverse deformations were less than one as were the majority of the slopes for strains other than the normal strain in the loaded direction. Visualization of the displacements and strains (e.g., Figs. 4–6) were informative as to the apparent similarities of the different methods of estimating parameters of interest.

Discussion and Conclusion

The FEM method predicted displacements in the loading direction that were very similar to those measured using the DVC method for the higher density femoral bone specimen. In the transverse directions, less accuracy was achieved. Results for the vertebral specimen the pattern were similar, but the predictions generally had poorer coefficients of determination than for the femoral case. This difference might be attributed to poorer accuracy of FEM for lower density tissue (larger voxels compared to

Table 2 Prediction of FEM results from DVC results (NS=not significant at $p<0.05$). "u" values are displacements and "ε" values are strains. Note that the ideal relationship is a slope of one with an intercept of zero.

	Femoral sample			Vertebral sample		
	R^2	Intercept	Slope	R^2	Intercept	Slope
$\mathbf{u}_x$	0.601	0.208	0.882	0.374	0.049	0.519
$\mathbf{u}_y$	0.293	−0.954	0.580	0.337	0.040	0.332
u_z	***0.970***	***0.145***	***0.981***	***0.905***	***0.079***	***0.934***
ε_{xx}	0.094	0.001	0.413	0.006	0.000	0.104
ε_{yy}	0.376	−0.001	1.171	0.126	0.000	0.407
ε_{zz}	***0.768***	***0.000***	***0.898***	***0.327***	***0.000***	***0.905***
ε_{xy}	0.071	−0.001	0.465	0.063	0.000	0.320
ε_{yz}	0.000	NS	NS	0.099	0.000	0.604
ε_{xz}	0.085	0.000	0.471	0.339	0.000	1.313

trabecular thickness [31–33]), the presence of modulus inhomogeneity in the specimens [13] and possible difficulty with resolving small trabecular elements using 35 micrometer voxels.

The presence of modulus inhomogeneity may affect deformations perpendicular to the loading direction (u_x,u_y). The specimens were loaded in the expected habitual functional load direction for the tissue specimens. Transverse trabeculae may have a lower modulus than trabeculae oriented in the habitual load direction [34,35], and would be expected to deform differently from the FEM prediction that used an assumption of uniform material properties. This could result in the models having a systematic error in prediction of the lateral expansion of the specimens relative to the experimental data. In the current case, the FEM models predicted smaller lateral deformation than measured using DVC (the slopes for the lateral deformation are smaller than one in Table 2 indicating that FEM predictions were smaller than DVC measurements). These results are consistent with the theoretical prediction that nonuniform material properties will have a significant effect upon the accuracy of FEM for cancellous bone [13].

Visualization of the vertical displacement (u_z) from the DVC, averaged FEM and direct FEM method (Fig. 4) for the best femoral displacement case (Table 2) provided some confidence that the methods can result in usefully comparable results. Visualization (Fig. 5) of the vertical normal strain (ε_{ZZ}) for the best femoral strain case (Table 2) demonstrates a limit of the DVC method in validating the predictions of FEM. The strain calculated from the DVC strain (Fig. 5, left panel) is similar to the strain calculated from average FEM displacement (Fig. 5, central panel) but both differ greatly from ε_{ZZ} calculated using unaveraged FEM displacement results (Fig. 5, right panel). Averaging the directly calculated FEM ε_{ZZ} using the same method as used to average the FEM displacements does not make the directly calculated FEM strains similar to the other strain measures (compare Fig. 6 with the left two panels of Fig. 5). These visualizations support the conclusion that the results of the DVC and FEM methods are similar at the level of the average displacements, but that the DVC method as used here is not able to test the predictions of trabecular

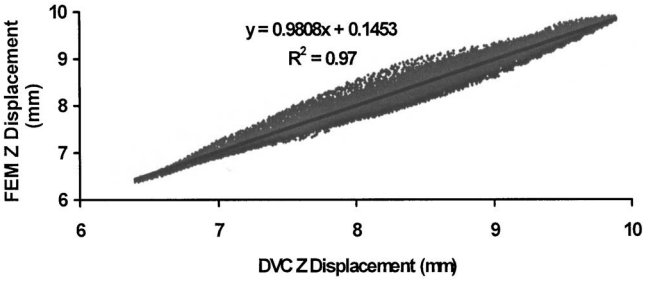

Fig. 2 Prediction of FEM vertical deformation by DVC for femoral sample

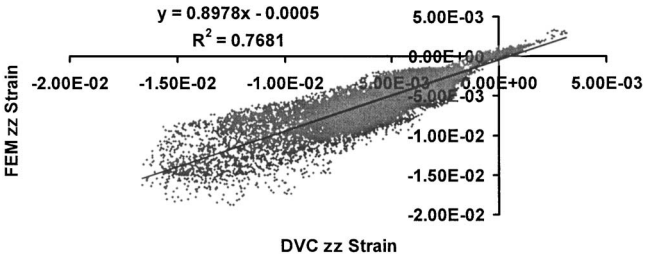

Fig. 3 Prediction of FEM vertical strain by DVC for femoral sample

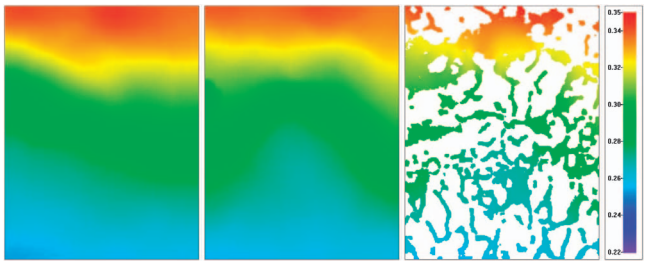

Fig. 4 Comparison of vertical displacement magnitude from DVC (left), averaged FEM (center), and actual FEM (right) for a coronal section through the femoral specimen. Colors represent displacement magnitude as presented in the key. The displacements are clearly similar and the averaged FEM displacements are comparable to those of the original FEM prediction. This shows both how the DVC and averaged FEM measures are similar and also that the averaging of the FEM was not so aggressive as to destroy its original character.

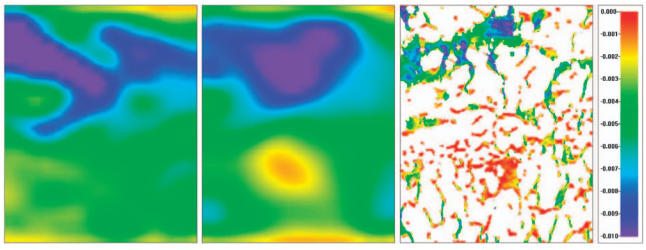

Fig. 5 Comparison of vertical strain (ε_{zz}) from DVC (left), strain calculatded from averaged FEM displacement (center), and actual FEM (right) for a coronal section through the femoral specimen. Colors represent strain presented in the key. The similarities between these strain panels are less than those for the displacement (Fig. 4).

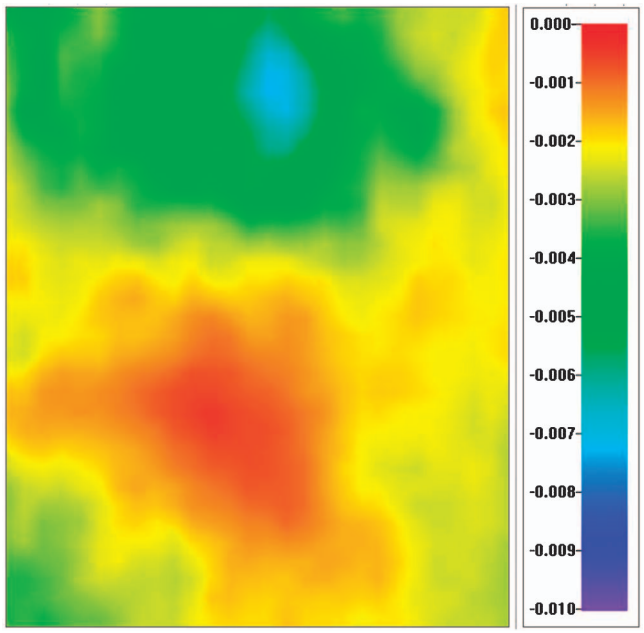

Fig. 6 Average of the vertical strain (ε_{zz}) from the right panel of Fig. 5. These results, directly averaged from the FEM calculation of strain, are distinct from strain calculated from averaged FEM or from DVC measured displacements. Causes of the differences are discussed in the body of the text.

level strain. This limitation arises from the use of DVC to track trabecular sized features of the deformed images. As a result, subtrabecular level predictions of FEM cannot be tested. This limitation is not in the DVC software, however, but rather is inherent to the scanner used in the current study. It is possible that improvements in scanner technology will eventually overcome this limitation.

This is the first report comparing the finite element estimated deformation and strain in cancellous bone to directly measured values of internal deformation and strain in three dimensions. Considering the current limitations of each technology, the good results for the main loading direction suggest that the DVC method could be used as a means to collect data to test the deformation estimates of the FEM method for cancellous bone.

Acknowledgment

NIH Grants AR40776 (D.P.F.), AR049343 (Y.N.Y.), Tait Smith, Ph.D., Lawrence Livermore National Laboratory.

Appendix A: Calculation of Values and Derivatives of Tricubic Interpolated Data

This appendix outlines steps used to efficiently code the derivatives of tricubic interpolated data used for the subvoxel resolution of displacement. The basic theory is discussed in [24], but our present implementation is different.

First, a matrix of the coefficients of the partial derivatives of the tricubic polynomial, evaluated at the eight locations $(x,y,z)=(0,0,0)$, (0,0,1), … (1,1,1), was built. This matrix contains only the coefficients generated by differentiation, not the polynomial fitting coefficients. Let us call this matrix M1. Next, invert M1 to define matrix $M2=(M1)^{-1}$ using the Gauss-Jordan elimination method. This matrix does not vary with respect to the data being interpolated, since it was generated from only the pure polynomial differentiation process.

Now we are faced with the problem of calculating the finite-difference derivatives. If we consider each of the eight vertices of the voxel space, we see that the 64 finite-difference derivatives are all linear functions of the 64 voxel values in the $4\times4\times4$ cube surrounding the voxel space and can be expressed as a matrix M3 multiplying the vector composed of the 64 voxel values.

Given the matrices, M2 and M3, the interpolation process works as follows:

(1) Arrange the voxel values at the 64 adjacent locations into a vector;
(2) multiply this vector by M3 to get a vector of the finite-difference derivatives of the eight vertices;
(3) multiply the finite-difference vector by M2 to get the 64 polynomial fitting coefficients;
(4) evaluate the 64 polynomial terms at the inter-voxel point of interest.

(Note: In the actual coding of the algorithm, the constant matrix [M2][M3] was precalculated and coded directly into the program as a fixed matrix.)

Appendix B: Strain Estimation

The result of the DVC process is a discrete displacement-vector field $\mathbf{d}(\mathbf{p})$, defined for successfully calculated reference points $\mathbf{p}$ in the specified grid. Following the method given in Bay et al. [24], a triquadratic interpolation of the discrete displacements is used first to smooth these displacements, then to estimate the strain tensor field from the smoothed displacement.

A Maclaurin series is fitted to neighboring reference points (typically 60) around each $\mathbf{p}$. For each reference point $\mathbf{p}_i$ neighboring $\mathbf{p}_0$, one can calculate the change in displacement ($\Delta\mathbf{d}$) as a function of change in position ($\Delta\mathbf{p}$) as:

$$\Delta\mathbf{d}(\Delta\mathbf{p}_i)=\mathbf{d}(\mathbf{p}_i)-\mathbf{d}(\mathbf{p}_0). \tag{B1}$$

Let $(\alpha_i,\beta_i,\gamma_i)$ represent the three components of $\Delta\mathbf{p}_i$ (distance from $\mathbf{p}_0$ to $\mathbf{p}_i$). The x-component of $\Delta\mathbf{d}(\Delta\mathbf{p}_i)$ can be estimated by the first ten terms of the three-dimensional Maclaurin series:

$$u(\alpha,\beta,\gamma)=U_0+\alpha\frac{\partial u}{\partial\alpha}+\beta\frac{\partial u}{\partial\beta}+\gamma\frac{\partial u}{\partial\gamma}+\frac{\alpha^2}{2}\frac{\partial^2 u}{\partial\alpha^2}+\frac{\beta^2}{2}\frac{\partial^2 u}{\partial\beta^2}+\frac{\gamma^2}{2}\frac{\partial^2 u}{\partial\gamma^2}+\alpha\beta\frac{\partial^2 u}{\partial\alpha\,\partial\beta}+\alpha\gamma\frac{\partial^2 u}{\partial\alpha\,\partial\gamma}+\beta\gamma\frac{\partial^2 u}{\partial\beta\,\partial\gamma}+\cdots \tag{B2}$$

These ten terms are fitted to the x-coordinate of $\Delta\mathbf{d}(\Delta\mathbf{p}_i)$ for the $\mathbf{p}_i$ neighboring $\mathbf{p}_0$, minimizing the least-squares error with steepest-decline search. The remaining terms of the series are ignored. Similarly, a ten term function $v(\alpha,\beta,\gamma)$ is fitted to the y-coordinate of $\Delta\mathbf{d}(\Delta\mathbf{p}_i)$ and, also, $w(\alpha,\beta,\gamma)$ is fitted to the z-coordinate of $\Delta\mathbf{d}(\Delta\mathbf{p}_i)$. In the first pass, the resulting constant terms (U_0,V_0,W_0) become the smoothed estimate of $\mathbf{d}(\mathbf{p}_0)$. In the second pass of the derivative process, the values of the three first-order terms

$$[S(\mathbf{p}_0)]=\begin{bmatrix}\frac{\partial u}{\partial\alpha} & \frac{\partial u}{\partial\beta} & \frac{\partial u}{\partial\gamma}\\ \frac{\partial v}{\partial\alpha} & \frac{\partial v}{\partial\beta} & \frac{\partial v}{\partial\gamma}\\ \frac{\partial w}{\partial\alpha} & \frac{\partial w}{\partial\beta} & \frac{\partial w}{\partial\gamma}\end{bmatrix} \tag{B3}$$

are used to estimate the linear (Cauchy) strain tensor at $\mathbf{p}_0$ as, $\varepsilon(\mathbf{p}_0)=\left(\frac{1}{2}\right)[S(\mathbf{p}_0)+S^T(\mathbf{p}_0)]$.

References

[1] Silva, M. J., Keaveny, T. M., and Hayes, W. C. 1997, "Load Sharing Between The Shell And Centrum In The Lumbar Vertebral Body," Spine, **22**(2): pp. 140–150.
[2] Silva, M. J., Keaveny, T. M., and Hayes, W. C., 1998, "Computed Tomography-Based Finite Element Analysis Predicts Failure Loads and Fracture Patterns for Vertebral Sections," J. Orthop. Res., **16**(3), pp. 300–308.

[3] Mizrahi, J., et al., 1993, "Finite-Element Stress Analysis of the Normal and Osteoporotic Lumbar Vertebral Body," Spine, **18**(14), pp. 2088–2096.
[4] Niebur, G. L., et al., 2000, "High-Resolution Finite Element Models With Tissue Strength Asymmetry Accurately Predict Failure of Trabecular Bone," J. Biomech., **33**(12), pp. 1575–1583.
[5] Liebschner, M. A., et al., 2003, "Finite Element Modeling of the Human Thoracolumbar Spine," Spine, **28**(6), pp. 559–565.
[6] Cody, D. D., et al., 1999, "Femoral Strength is Better Predicted by Finite Element Models Than QCT and DXA," J. Biomech., **32**(10), pp. 1013–1020.
[7] Cody, D. D., et al., 2000, "Femoral Structure and Stiffness in Patients With Femoral Neck Fracture," J. Orthop. Res., **18**(3), pp. 443–448.
[8] Cody, D. D., et al., 2000, "Short Term in Vivo Precision of Proximal Femoral Finite Element Modeling," Ann. Biomed. Eng., **28**(4), pp. 408–414.
[9] Crawford, R. P., Cann, C. E., and Keaveny, T. M., 2003, "Finite Element Models Predict in Vitro Vertebral Body Compressive Strength Better Than Quantitative Computed Tomography," Bone (N.Y.), **33**(4), pp. 744–750.
[10] Crawford, R. P., Rosenberg, W. S., and Keaveny, T. M., 2003, "Quantitative Computed Tomography-Based Finite Element Models of the Human Lumbar Vertebral Body: Effect of Element Size on Stiffness, Damage, and Fracture Strength Predictions," J. Biomech. Eng., **125**(4), pp. 434–438.
[11] Fyhrie, D. P., et al., 2000, "Shear Stress Distribution in the Trabeculae of Human Vertebral Bone," Ann. Biomed. Eng., **28**(10), pp. 1194–1199.
[12] Hou, F. J., et al., 1998, "Human Vertebral Body Apparent and Hard Tissue Stiffness," J. Biomech., **31**(11), p. 1009–1015.
[13] Jaasma, M. J., et al., 2002, "Biomechanical Effects of Intraspecimen Variations in Tissue Modulus for Trabecular Bone," J. Biomech., **35**(2), pp. 237–246.
[14] Van Rietbergen, B., et al., 1999, "Tissue Stresses and Strain in Trabeculae of a Canine Proximal Femur can be Quantified From Computer Reconstructions," J. Biomech., **32**(4), pp. 443–451.
[15] van Rietbergen, B., 2001, "Micro-FE Analyses of Bone: State of the art," Adv. Exp. Med. Biol., **496**, pp. 21–30.
[16] van Rietbergen, B., et al., 2002, "High-Resolution MRI and Micro-FE for the Evaluation of Changes in Bone Mechanical Properties During Longitudinal Clinical Trials: Application to Calcaneal Bone in Postmenopausal Women After one Year of Idoxifene Treatment," Clin. Biomech. (Bristol, Avon), **17**(2), pp. 81–88.
[17] Yeni, Y. N. and Fyhrie, D. P., 2001, "Finite Element Calculated Uniaxial Apparent Stiffness is a Consistent Predictor of Uniaxial Apparent Strength in Human Vertebral Cancellous Bone Tested With Different Boundary Conditions," J. Biomech., **34**(12), pp. 1649–1654.
[18] Yeni, Y. N., et al., 2003, "Trabecular Shear Stresses Predict in Vivo Linear Microcrack Density but not Diffuse Damage in Human Vertebral Cancellous Bone," Ann. Biomed. Eng., **31**(7), pp. 726–732.
[19] Ulrich, D., et al., 1999, "Load Transfer Analysis of the Distal Radius From in-Vivo High-Resolution CT-Imaging," J. Biomech., **32**(8), pp. 821–828.
[20] Huiskes, R., 1982, "On the Modelling of Long Bones in Structural Analyses," J. Biomech., **15**(1), pp. 65–69.
[21] Guo, X. E., et al., 2002, "Quantification of a rat Tail Vertebra Model for Trabecular Bone Adaptation Studies," J. Biomech., **35**(3), pp. 363–368.
[22] Akhter, M. P., et al., 1992, "Characterization of in Vivo Strain in the rat Tibia During External Application of a Four-Point Bending Load," J. Biomech., **25**(10), pp. 1241–1246.
[23] Bay, B. K., 1995, "Texture Correlation: A Method for the Measurement of Detailed Strain Distributions Within Trabecular Bone," J. Orthop. Res., **13**, pp. 258–267.
[24] Bay, B. K., et al., 1999, "Digital Volume Correlation: Three-Dimensional Strain Mapping Using X-Ray Tomography," Exp. Mech.," **39**(3), pp. 217–226.
[25] Smith, T., Bay, B., and Rashid, M., 2002, "Digital Volume Correlation Including Rotational Degrees of Freedom During Minimization," Exp. Mech., **42**(3), pp. 272–278.
[26] Odgaard, A., Hvid, I., and Linde, F., 1989, "Compressive Axial Strain Distributions in Cancellous Bone Specimens," J. Biomech., **22**(8-9), pp. 829–835.
[27] Nicolella, D. P., et al., 2001, "Machine Vision Photogrammetry: a Technique for Measurement of Microstructural Strain in Cortical Bone," J. Biomech., **34**(1), pp. 135–139.
[28] Reimann, D. A., et al., 1997, "A Cone Beam Computed Tomography System for True 3D Imaging of Specimens," Appl. Radiat. Isot., **48**(10-12), pp. 1433–1436.
[29] Luenberger, D. G., 1973, *Introduction to Linear and Nonlinear Programming*, Addison-Wesley, Reading.
[30] Malvern, L. E., 1969, *Introduction to the Mechanics of a Continuous Medium*, Prentice-Hall, Inc., Englewood Cliffs.
[31] Niebur. G. L., et al., 1999, "Convergence Behavior of High-Resolution Finite Element Models of Trabecular Bone," J. Biomech. Eng., **121**(6), pp. 629–635.
[32] Charras, G. T. and Guldberg, R. E., 2000, "Improving the Local Solution Accuracy of Large-Scale Digital Image-Based Finite Element Analyses," J. Biomech., **33**(2), pp. 255–259.
[33] Guldberg, R. E., Hollister, S. J., and Charras, G. T., 1998, "The Accuracy of Digital Image-Based Finite Element Models," J. Biomech. Eng., **120**(2), pp. 289–295.
[34] Rho, J. Y., et al., 2002, "Microstructural Elasticity and Regional Heterogeneity in Human Femoral Bone of Various Ages Examined by Nano-Indentation," J. Biomech., **35**(2), pp. 189–198.
[35] Rho, J. Y., Kuhn-Spearing, L., and Zioupos, P., 1998, "Mechanical Properties and the Hierarchical Structure of Bone," Med. Eng. Phys., **20**(2), pp. 92–102.